



Teleseismic finite-fault inversion of two $M_w = 6.4$ earthquakes along the East Anatolian Fault Zone in Turkey: the 1998 Adana and 2003 Bingöl earthquakes

Murat Utkucu¹ · Emrah Budakoğlu¹ · Meltem Çabuk¹

Received: 22 November 2017 / Accepted: 16 November 2018 / Published online: 24 November 2018
© Saudi Society for Geosciences 2018

Abstract

The East Anatolian Fault Zone is a continental transform fault accommodating westward motion of the Anatolian fault. This study aims to investigate the source properties of two moderately large and damaging earthquakes which occurred along the transform fault in the last two decades using the teleseismic broadband P and SH body waveforms. The first earthquake, the 27 June 1998 Adana earthquake, occurred beneath the Adana basin, located close to the eastern extreme of Turkey's Mediterranean coast. The faulting associated with the 1998 Adana earthquake is unilateral to the NE and confined to depths below 15 km with a length of 30 km along the strike (53°) and a dipping of 81° SE. The fixed-rake models fit the data less well than the variable-rake model. The main slip area centered at depth of about 27 km and to the NE of the hypocenter, covering a circular area of 10 km in diameter with a peak slip of about 60 cm. The slip model yields a seismic moment of 3.5×10^{18} N-m ($M_w \cong 6.4$). The second earthquake, the 1 May 2003 Bingöl earthquake, occurred along a dextral conjugate fault of the East Anatolian Fault Zone. The preferred slip model with a seismic moment of 4.1×10^{18} N-m ($M_w \cong 6.4$) suggests that the rupture was unilateral toward SE and was controlled by a failure of large asperity roughly circular in shape and centered at a depth of 5 km with peak displacement of about 55 cm. Our results suggest that the 1998 Adana earthquake did not occur on the mapped Göksun Yakapınar Fault Zone but rather on a SE dipping unmapped fault that may be a split fault of it and buried under the thick (about 6 km) deposits of the Adana basin. For the 2003 Bingöl earthquake, the final slip model requires a rupture plane having 15° different strike than the most possible mapped fault.

Keywords The 1998 Adana earthquake · The 2003 Bingöl earthquake · The East Anatolian Fault Zone · Finite-fault inversion · Lower crustal earthquake · Eastern Turkey

Introduction

In response to the northward convergence of Arabian and African plates with respect to the stable Eurasian plate, the Anatolian plate moves west while deformation associated with the convergence is conveyed to the Caucasian thrust zones in eastern Turkey (Fig. 1) (McClusky et al. 2000; Hubert-Ferrari et al. 2003; Vernant et al. 2004; Reilinger et al. 2006). North and East Anatolian Fault Zones (NAFZ

and EAFZ) are continental strike-slip faults that accommodate westward motion of the Anatolian Plate with sporadic occurrence of large destructive earthquakes (Barka and Kadinsky-Cade 1988; Ambraseys 1989; Hubert-Ferrari et al. 2003; Şengör et al. 2005; Ambraseys 2009; Bulut et al. 2012; Duman and Emre 2013).

The EAFZ is a sinistral fault and extends between Karhova, where it meets with the NAFZ, and Antakya, where it connects with the Dead Sea Fault (Fig. 1) (Barka and Kadinsky-Cade 1988; Duman and Emre 2013). Additionally, it has a branch, called the northern branch, and separates from the main fault in the immediate west of the Çelikhan and extends through Adana basin to join with Misis Kyrenia Fault Zone beneath the easternmost Mediterranean Sea (Westaway 2004; Duman and Emre 2013; Seyrek et al. 2014). GPS studies indicate 9–10 mm/year

✉ Murat Utkucu
mutkucu@sakarya.edu.tr

¹ Department of Geophysical Engineering, Sakarya University, 54187 Serdivan, Sakarya, Turkey

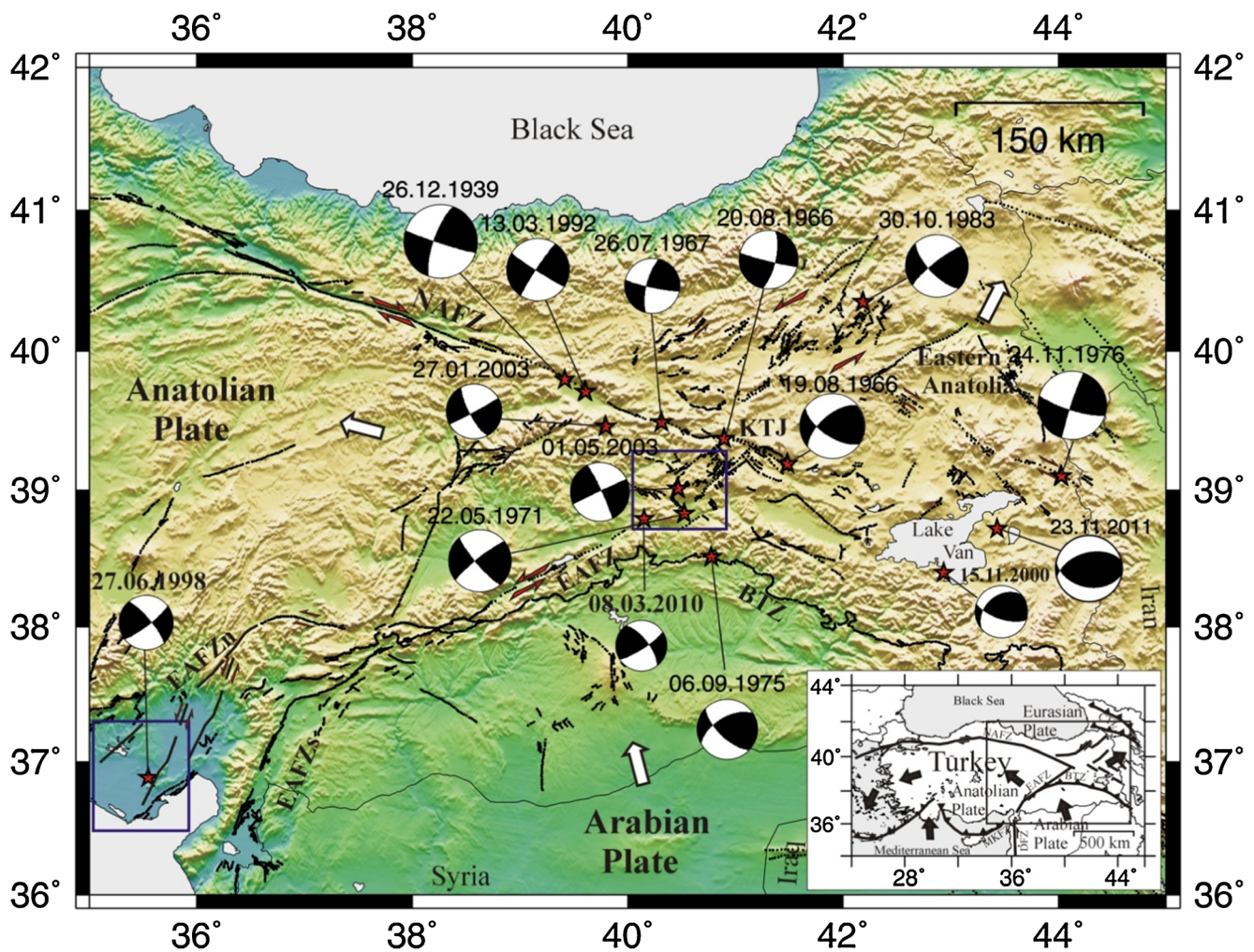


Fig. 1 Map showing major tectonic elements of Turkey (inset) and seismotectonic of eastern Turkey. Red stars indicate epicenter of the earthquakes with magnitude $M_S \geq 6.0$ occurred in the region (faults are compiled from Şaroğlu et al. 1992 and Duman and Emre 2013 while source mechanisms are taken from McKenzie 1972, Toksöz et al. 1978, Taymaz et al. 1991, Pınar 1995, Aktar et al. 2000, Pınar et al. 2007, and

Global Centroid Moment Tensor (GCMT) catalog). Large arrows indicate direction of relative plate motions. Blue-outlined rectangles enclose the map areas shown in Figs. 3 and 8. NAFZ North Anatolian Fault Zone, EAFZ East Anatolian Fault Zone, BTZ Bitlis Thrust Zone, KTJ Karlhova Triple Junction, DSZ Dead Sea Fault Zone, MKFZ Misis Kyrenia Fault Zone

slip rate for the EAFZ (McClusky et al. 2000; Reilinger et al. 2006), about one third of which is shared by the northern strand after the bifurcation (Westaway 2004; Altunel et al. 2009; Mahmoud et al. 2013; Duman and Emre 2013). Although the EAFZ was relatively quiescent in the twentieth century in contrast to the NAFZ that ruptured along most of its length, it had been very active in the nineteenth century as indicated by historical seismicity studies (Ambraseys 1989; Nalbant et al. 2002). Modeling using the principle of elastic fracture mechanics revealed that the seismic activity could have switched between the NAFZ and the EAFZ as observed in the historical record (Hubert-Ferrari et al. 2003). If so, it is not farfetched to deduce relatively high seismic activity along the EAFZ in the future as indicated by the recent studies (Nalbant et al. 2002; Duman and Emre 2013). Therefore, understanding of both fault zone structure and occurrence of

earthquakes along the EAFZ as in the present study is considered to be significant (Nalbant et al. 2005).

Finite-fault inversions of earthquakes are important in seismotectonic studies because they provide valuable information such as spatial distribution of co-seismic slip at depth, the rupture extends for understanding of fault segmentation, and detailed source models for forward prediction of near-source ground motions (Wald et al. 1991; Wald and Heaton 1994; Mendoza 1995). This information would especially be significant for the earthquakes that do not produce clear surface ruptures or with no surface ruptures. The purpose of this study is to obtain finite-fault, co-seismic rupture models of two moderately large $M_w = 6.4$ Anatolian earthquakes that occurred along the EAFZ from the broad band teleseismic body waveforms. These earthquakes are the 27 June 1998 Adana and the 1 May 2003 Bingöl earthquakes (Fig. 1). No

finite-fault rupture models from teleseismic velocities have been published so far for both studied earthquakes. Therefore, finite-fault rupture models would be important to understand rupture properties of these earthquakes that produced no surface ruptures.

Data

We invert teleseismic broadband *P* and *SH* velocity waveforms retrieved from the IRIS Data Management Centre to model co-seismic slip distributions for both the 1998 Adana and 2003 Bingöl earthquakes. After the correction of the instrument responses, the data are bandpass filtered using corner frequencies at 0.01 to 0.5 Hz. The data are resampled with time intervals of 0.25 and 0.20 s for the 1998 Adana and 2003 Bingöl earthquakes, respectively. A total of 25 *P* and 5 *SH* waveforms recorded at teleseismic distances between 31° and 87° are included in the inversion of the 1998 Adana earthquake while 18 *P* and 13 *SH* waveforms recorded at teleseismic distances between 29° and 91° are used in the inversion of the 2003 Bingöl earthquake. The selection of the epicentral ranges is due to minimizing upper mantle distortions and core–mantle boundary diffractions in the waveforms. Considering the size and the finite-fault model parameterization of the earthquakes (Fig. 2), record lengths of 30 s

for the 1998 Adana earthquake and 20 s (for *P* waves) and 25 s (for *SH* waves) for the 2003 Bingöl earthquake are chosen.

Method

A finite-fault waveform inversion methodology developed by Hartzell and Heaton (1983) is utilized in order to obtain the slip distribution of both earthquakes from the broadband teleseismic *P* and *SH* velocity waveforms. The sources of the earthquakes are represented by model fault planes (Fig. 2), the dimensions and source parameters of which are defined according to the available information such as magnitude, aftershock distribution, and strike, dip, and rake angles from the previous point source modeling studies as well as from the available geological studies. The model fault planes are then divided into a number of subfaults for the spatial distribution of slip and are embedded in the crustal structure of the source regions regarding their assigned geometries. Radial propagation of the rupture from the hypocenter is simulated by evenly placed point sources over the model fault planes with an initially defined rupture velocity.

The point source responses are calculated using Generalized Ray Theory (Langston and Helmberger 1975) with a crustal velocity structure adopted for each earthquake. After being appropriately lagged by the rupture delay time, the point source responses are summed to construct subfault synthetic seismograms (Green’s functions) for each station included in the inversion. Attenuation is accounted for by convolving the synthetic seismograms with a constant frequency-dependent attenuation operator, t^* (Choy and Cormier 1986). In the present study, the synthetic *P* and *SH* waveforms are convolved with a constant t^* of 0.7 and 4 s, respectively.

To compute the subfault synthetics, a slip rise-time function and a rupture velocity must be defined. A time window approach (Hartzell and Heaton 1983; Wald and Heaton 1994; Mendoza 1995) is incorporated in the modeling to allow variable slip rise-time and the rupture velocity over the model faults. Although the rupture velocity is allowed to vary in an assigned range, an initial maximum rupture velocity that describes the earliest possible failure time of each point over the model fault plane must be defined.

The subfault synthetic records and the observed records define an over determined system of linear equations of the form $Ax = b$, where A is the matrix of synthetics, b is the data vector, and x is the solution vector including slip weights to be given each subfault so that the synthetics fit the observed data. The solution vector, x , is solved by using a Householder least squares inversion method (Lawson and Hanson 1974) that constrains each value of the solution vector to be greater than or equal to zero. To find a finite-fault slip model with a smooth distribution of slip and with minimum seismic moment, smoothing, and moment minimization constraints are also

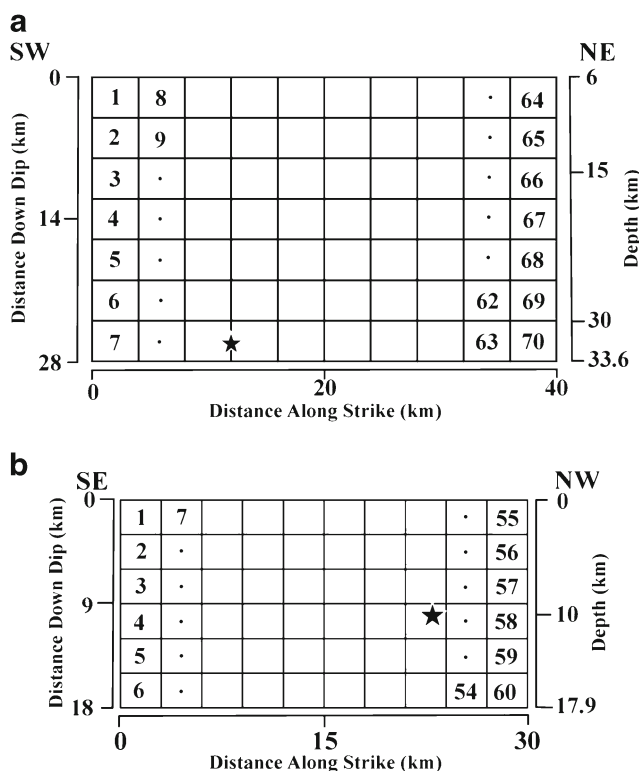


Fig. 2 a Parameterizations of the model fault planes used in the study for the 1998 Adana and b the 2003 Bingöl (bottom) earthquakes. Solid stars represent the hypocenters

imposed on the inversion (see Hartzell and Heaton 1983 and Wald and Heaton 1994 for further details of the method).

The 27 June 1998 Adana earthquake ($M_w = 6.4$)

On 27 June 1998, a moderately large earthquake hit the Adana basin located along Turkey's Mediterranean coast with heavy damage and fatalities (Figs. 1 and 3). Seismotectonics of this region is controlled by the convergence of the Anatolian, African, and Arabian plate and the region represents a distributed plate boundary zone (Ergin 1999; Aktar et al. 2000; Westaway 2004; Seyrek et al. 2014). Collision regime between the Arabian and Anatolian plates in the east of the source region turns into a subduction-dominated regime between the African and Anatolian plates in the west. The relative motion of the plates is mainly eliminated by two sinistral

faults, namely the EAFZ and Dead Sea Fault (Fig. 1) (Westaway 2004; Duman and Emre 2013; Seyrek et al. 2014). The Adana basin comprises complex tectonic features related to interaction processes among the three plates and has been developed as a left lateral diffuse shearing zone as confirmed by the stress-tensor analysis of the earthquakes which occurred in the basin and its vicinity (Ergin et al. 2004). Göksun Yakapınar Fault Zone (GYFZ), Yumurtalık Fault Zone (YFZ), and Kozan Fault Zone are the left-lateral faults developed within the basin (Figs. 1 and 3). The GYFZ has been considered a part of the northern branch of the EAFZ and joins Misis Kyrenia Fault Zone beneath the Mediterranean Sea (Karig and Kozlu 1990; Westaway 2004; Burton-Ferguson et al. 2005; Aksu et al. 2005, 2014; Derman and Gürbüz 2007; Emre et al. 2013; Duman and Emre 2013; Seyrek et al. 2014; Walsh-Kennedy et al. 2014).

The source parameters of the earthquake are summarized in Table 1. The fault plane solution indicates left-lateral strike

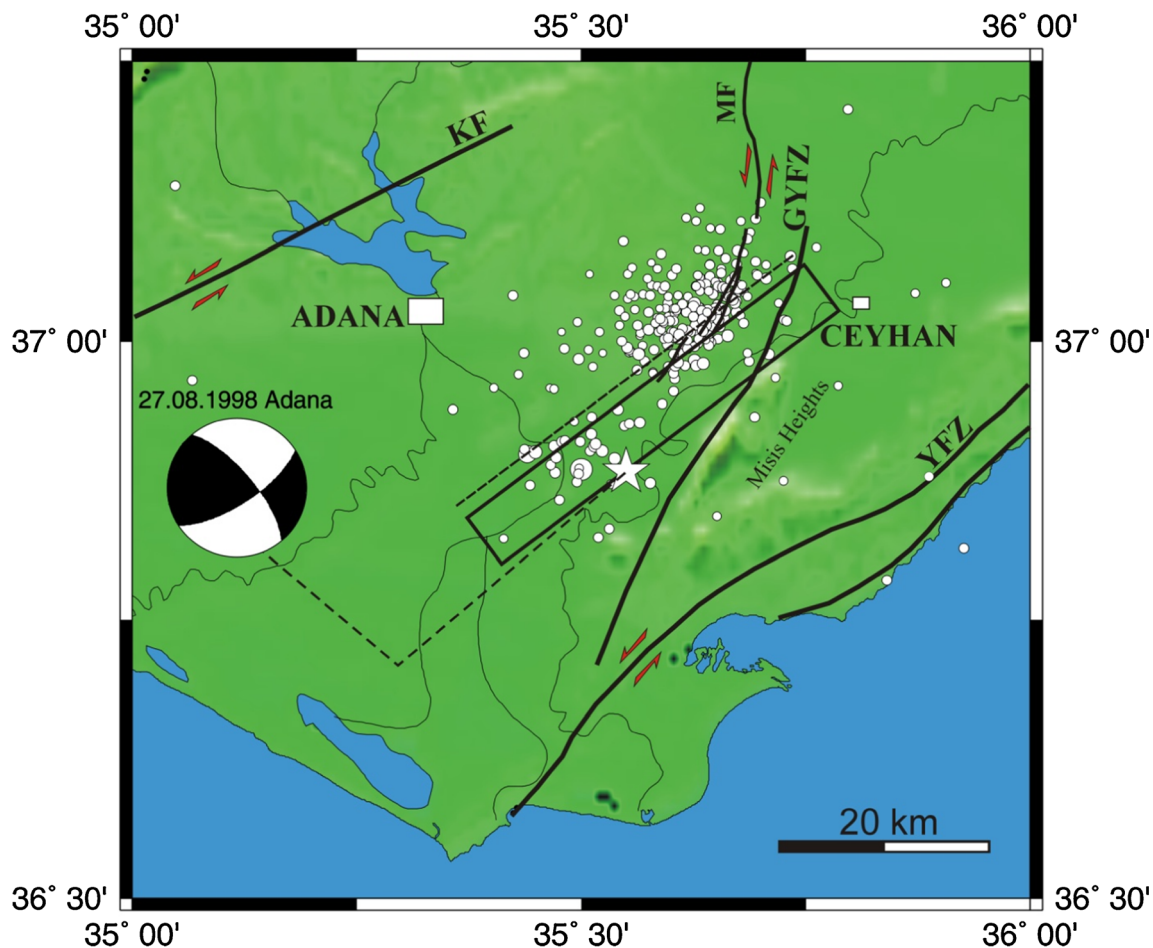


Fig. 3 Location map showing the epicenter (white star), the aftershocks (white circles), and fault plane solution of the 27 June 1998 Adana earthquake. Blue line indicates approximate extent of the surface perturbations observed after the earthquake. Solid rectangle denotes the surface projection of the model fault plane shown in Fig. 2. Broken line shows intersection of the model fault plane with the surface. GYFZ, KF,

MF, and YFZ indicate Göksun Yakapınar Fault Zone, Kozan Fault, Misis Fault, and Yumurtalık Fault Zone, respectively. The faults are compiled from Karig and Kozlu (1990), Westaway (2004), Burton-Ferguson et al. (2005), Aksu et al. (2005), Derman and Gürbüz (2007), Emre et al. (2013), and Walsh-Kennedy et al. (2014)

Table 1 The source parameters of the 27 June 1998 Adana earthquake obtained by previous inversion studies and the seismological centers

	USGS		GCMT		Aktar et al. (2000)		Arpacioğlu (2000)
Latitude (°)	36.94		36.87		36.53		–
Longitude (°)	35.30		35.58		35.33		–
Depth (km)	14		29.5		32		18
M_0 ($\times 10^{18}$ N-m)	3.96		2.96		3.63		2.63
M_w	6.3		6.2		6.2		6.2
Strike (°)	323	52	321	53	65 ^a	50 ^b	52 ^b
Dip (°)	77	81	75	81	90	85	75
Rake (°)	170	13	121	15	5	10	22

^a From the *P* wave first motion polarities^b From the inversion of the teleseismic waveforms

slip faulting with a minor reverse component. The earthquake occurred in the middle of temporal Cilician Network (comprising 17 seismograph stations), which had been operating since 1992 (Ergin et al. 2004). Thus, the data provided by the network, which was further enhanced by four additional seismographs for monitoring the aftershocks following the mainshock, led to well-constrained determination of both the mainshock and the aftershock locations, revealing an unusual feature of the earthquake as a crustal event. The mainshock hypocenter was located at a depth of 32 km while the aftershocks covered a depth range of 17–37 km, comprising two distinct clusters (Aktar et al. 2000; Ergin et al. 2004). Besides, Harvard CMT solution indicates a centroid depth at 29.5 km (Table 1). The fact that no surface rupture was observed but only some surface perturbations along the western bank of Ceyhan River after the earthquake also supports a faulting deep in the crust. The surface perturbations were most likely related to the lateral spreading due to liquefaction. The earthquake was claimed to occur on the GYFZ whose mapped trend roughly coincides with the aftershock elongation and the nodal plane striking NE–SW from the fault plane solution (Aktar et al. 2000) (Fig. 3).

Model fault parameterization

A rectangular fault plane 40-km long and 28-km wide in down dip is used to represent the rupture area of the Adana earthquake (Figs. 2 and 3). A broad fault plane is used to confine deep mainshock and aftershock hypocenters and to allow, if any, possible shallow slip contribution to be included in the modeling. The fault plane is discretized into 70 square subfaults (Fig. 2). Note that both the mainshock hypocenter and the aftershocks require the mapped GYFZ to dip toward NW, but the fault plane solutions require a rupture plane dipping SE. Adding that there is about 15° difference between the strike of the mapped GYFZ and the strike value resulted from the fault plane solutions (Table 1), we deduced that the earthquake possibly did not occur on the mapped GYFZ but rather

on an unmapped, SE-dipping splay fault. This fault could be buried beneath the thick sedimentary layers of the Adana basin. The fault plane strikes 53° and dips 81° toward SE (Table 1). The rake is allowed to vary between 0° and 90°. The fault plane is embedded in the source region such that it extends at depths between 6 and 33.6 km. The hypocenter location of the Cilician Network (36.53° N, 35.33° E; depth = 32 km) is used as a rupture initiation point. A rupture velocity of 2.7 km/s is utilized in the modeling. The subfault slip-time function is modeled using four time windows; displacement rise time of each represented by isosceles triangle of 0.3 s rise and fall. Each time window is delayed 0.6 s from the previous one, thus, allowing total rise time of 2.4 s for each point across the model fault. The crustal velocity structure after Aktar et al. (2000) is utilized in the calculations of the synthetic waveforms (Table 2).

Different fault model parameterizations are also tried (Table 3). Fault models having strike and dip values of 50° and 85°, respectively, fixed rake angles of 0°, 5°, 10°, and 15°, a hypocenter depth of 30 km as well as a NW-dipping fault plane (representing the rupture on the mapped GYFZ) are all tried. Also, a smaller (40 km \times 24 km) and shallower fault model (covering depths between 1 and 24.7 km) having strike and dip value of 53° and 81°, respectively, and a hypocenter depth of 22 km is tested.

Table 2 Crustal velocity structure utilized in the inversion of the 27 June 1998 Adana earthquake (after Aktar et al. 2000)

Thickness (km)	V_p (km/s)	V_s (km/s)	ρ (g/cm ³)
2	4.51	3.39	2.66
2	5.02	3.77	2.75
8	6.07	4.62	2.88
16	6.15	4.65	3.30
4	6.60	4.96	3.40
–	7.82	5.87	3.50

Table 3 Inversion results for different fault model parameterizations for the 1998 Adana earthquake

Model	Fault dimension (km × km)	Subfault number	Strike (°)	Dip (°)	Rake (°)	Depth extent (km)	Hypocenter depth (km)	Latitude–longitude (°)	$\ \mathbf{b} - \mathbf{Ax}\ $	M_0 ($\times 10^{18}$ N-m)
IRA1	40 × 28	70	53	81	0–90	6–33.6	32	36.53N–35.33E	19.473	3.49
IRA2	40 × 28	70	53	81	5	6–33.6	32	36.53N–35.33E	19.802	2.77
IRA3	40 × 28	70	53	81	15	6–33.6	32	36.53N–35.33E	20.160	2.07
IRA4	40 × 28	70	53	81	10	6–33.6	32	36.53N–35.33E	19.948	2.16
IRA5	40 × 28	70	53	81	0	6–33.6	32	36.53N–35.33E	20.048	2.93
IRA6	40 × 28	70	50	85	0–90	6–33.8	32	36.53N–35.33E	19.733	3.16
IRA7	40 × 28	70	53	81	0–90	6–33.6	30	36.53N–35.33E	19.598	3.61
IRA8	40 × 24	60	53	81	5	1–24.7	22	36.53N–35.33E	21.123	1.55
IRA9	40 × 28	70	218	81	0–90	6–33.6	32	36.53N–35.33E	21.968	7.91

The value of $\|\mathbf{b} - \mathbf{Ax}\|$ indicates the Euclidean norm of the misfit between the synthetic and the observed data

Inversion results

Inversion results are listed in Table 3. The best-fitting solution is found for a fault model covering depths between 6 and 33.6 km, striking 53°, dipping 81° SE and having a rupture initiation point at a depth of 32 km (Model IRA1 in Table 3). It is determined that a slip model with variable rake fits the data better than a slip model with fixed rake (Fig. 4). A shallow rupture assumption (a fault model cutting only the upper crust with depth range from 1 to 24.7 km and a hypocentral depth of 22 km) gave poor fit to the data (Model IRA8 in Table 3), which supports the assertion that the earthquake was a lower crust event (Aktar et al. 2000; Ergin et al. 2004). NW-dipping fault plane (Model IRA9 in Table 3) also gave poor fit to the data. This supports the idea that the earthquake occurred on an unmapped, SE-dipping fault, which could be a split fault of the GYFZ (Fig. 3). The best-fitting solution suggest that the rupture is virtually confined to the lower crust (below depth of 15 km), mainly proceeded to the NE from the hypocenter and covers a length of 30 km (Fig. 5). The synthetic and observed

data are compared for the preferred inversion in Fig. 6. The slip model yields a peak slip of about 60 cm and a seismic moment of 3.5×10^{18} N-m ($M_w \cong 6.4$). A rupture along a SE-dipping split fault could be better imagined in Fig. 7.

The 1 May 2003 Bingöl earthquake ($M_w = 6.4$)

The 1 May 2003 Bingöl earthquake occurred on a conjugate fault related to the EAFZ within the Karlıova Triple Junction area where the EAFZ and NAFZ meet (Figs. 1 and 8) (Emre et al. 2003; Dirik et al. 2003; Milkereit et al. 2004). In the triangular region bounded by the NAFZ and the EAFZ, many conjugate or secondary fault zones such as left-lateral Sancak–Uzunpınar Fault Zone and Kilisedere Fault and right-lateral Sudüğünü Fault Zone (SUFZ) and Bingöl–Karakoçan Fault Zone related to the connection of these continental transforms have developed. The earthquake caused hundreds of fatalities, injuries, and collapse of buildings (Yalçınkaya 2003; Dirik et al. 2003; Turer et al. 2004).

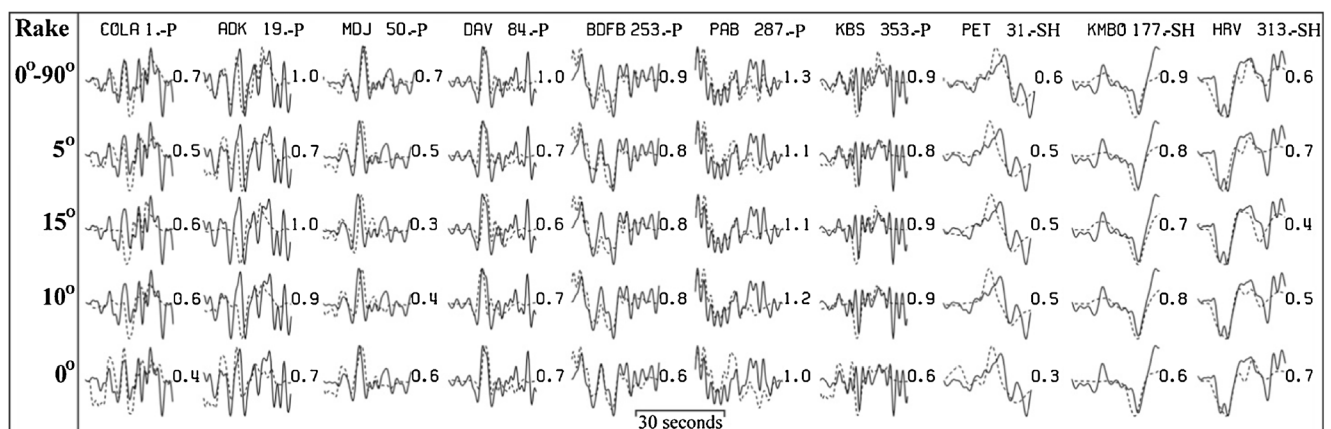
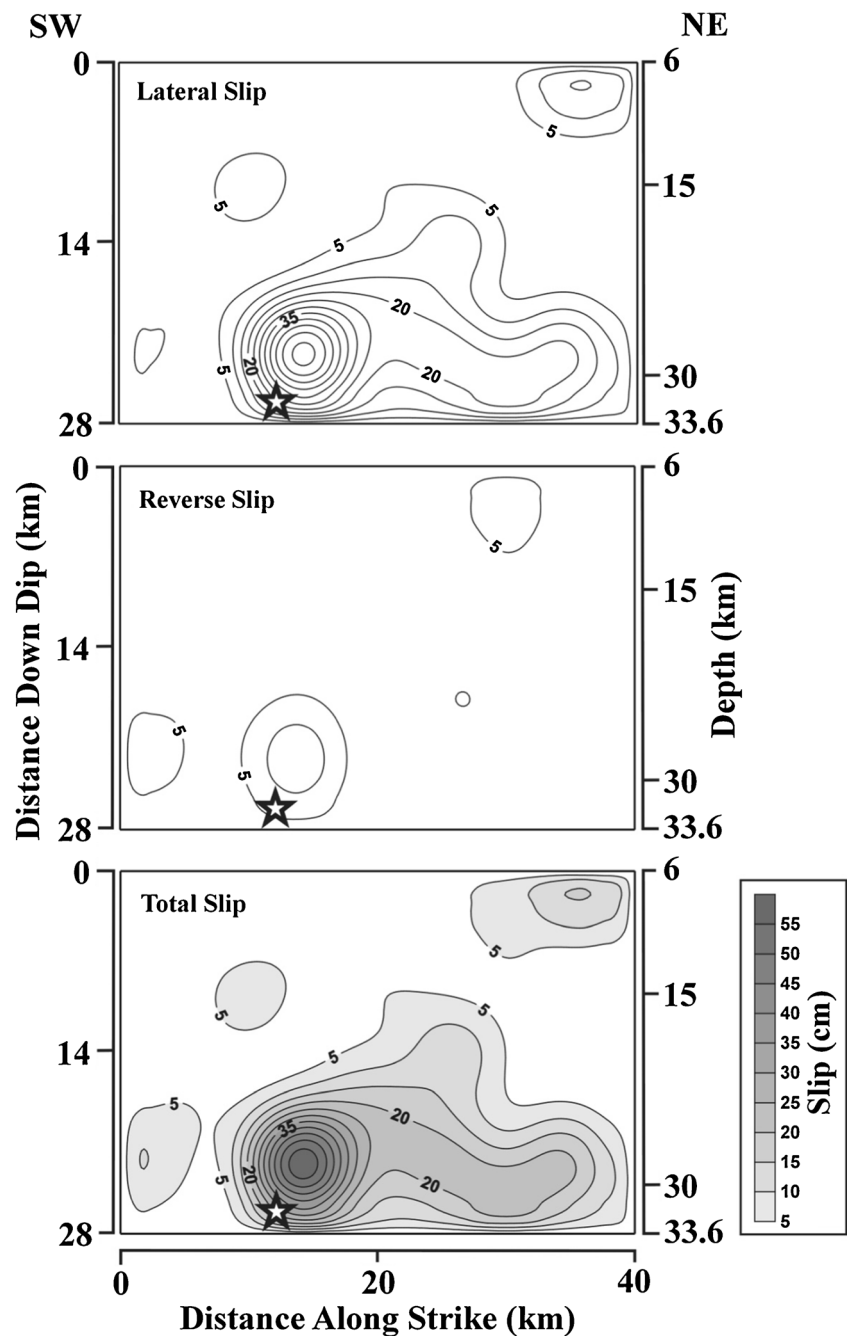


Fig. 4 Comparison of the synthetic waveforms (dashed), calculated for different rake angles at selected stations, with the observed waveforms (solid). Station names, azimuths, and waveform phases are given above

the columns and the numbers to the right of the observed–synthetic seismogram pairs are synthetic-to-observed (peak amplitude) ratios

Fig. 5 Preferred co-seismic slip distribution for the 27 June 1998 Adana earthquake obtained from the finite-fault analysis in the study. Slips are contoured at 5-cm intervals and only slips larger than 5 cm are contoured. The open star denotes the hypocenter



The earthquake did not generate clear and continuous surface ruptures (Dirik et al. 2003; Emre et al. 2003; Lazios et al. 2004). Dextral displacements rarely exceeded 20 cm along the observed surface ruptures (Lazios et al. 2004). The surface ruptures extended in NW–SE direction as a diffuse zone around the SUFZ with reported enechelon pattern which was put forward as an evidence of the earthquake rupture reaching to the surface. Nevertheless, Emre et al. (2003) did not refer to them as surface rupture at all and could not be able to assign the

source fault from the field observations alone. The source parameters of the earthquake are summarized in Table 4. Although it is not certain, the seismological data also suggests the SUFZ as the most probable source fault. The source parameters compiled in Table 4 and pattern of the well-located aftershocks (Fig. 8; Milkereit et al. 2004) require a fault rupture striking NW–SE with dextral sense of motion. However, it should be noted that general strike of the SUFZ differs about 15° from the strike required by the seismological data.

Fig. 6 Comparison of the predicted *P* and *SH* waveforms calculated for the slip model shown in Fig. 5 (dashed) with the observed waveforms (solid). Station names, azimuths, and waveform phases are given above each observed-synthetic seismogram pairs and the numbers to the right of each pair indicate synthetic-to-observed (peak amplitude) ratios

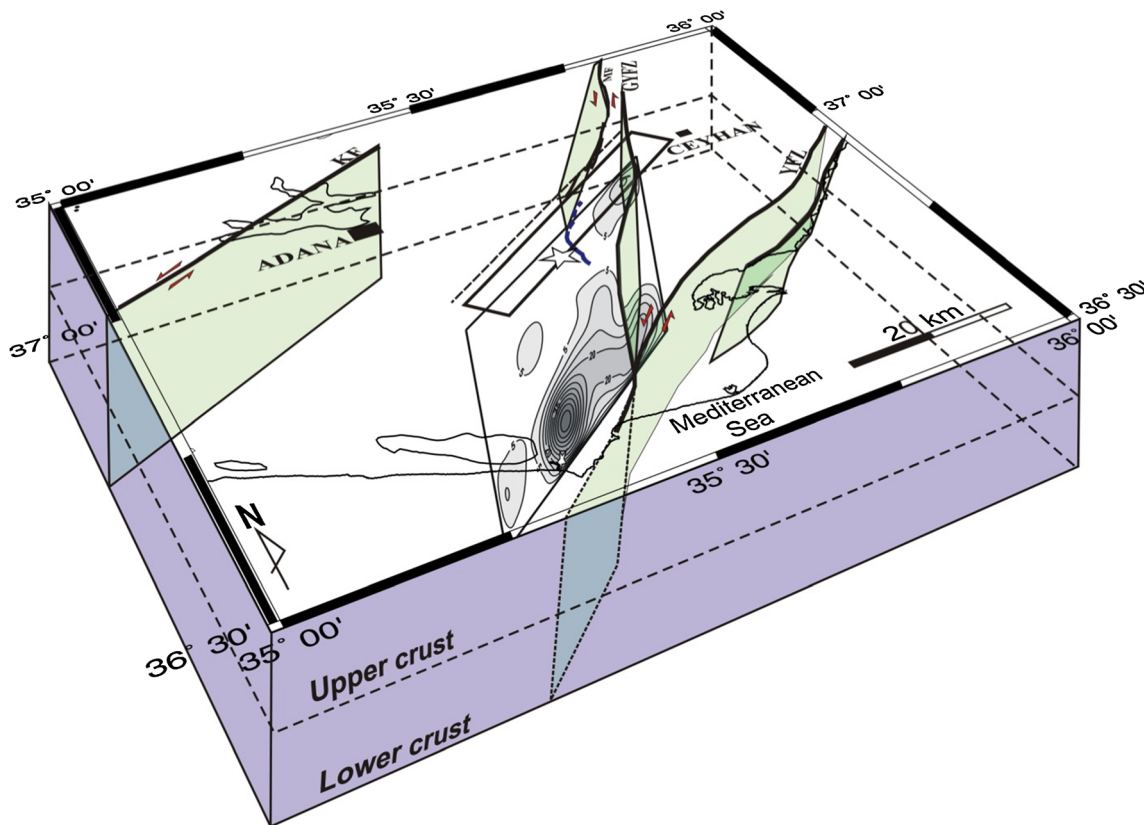
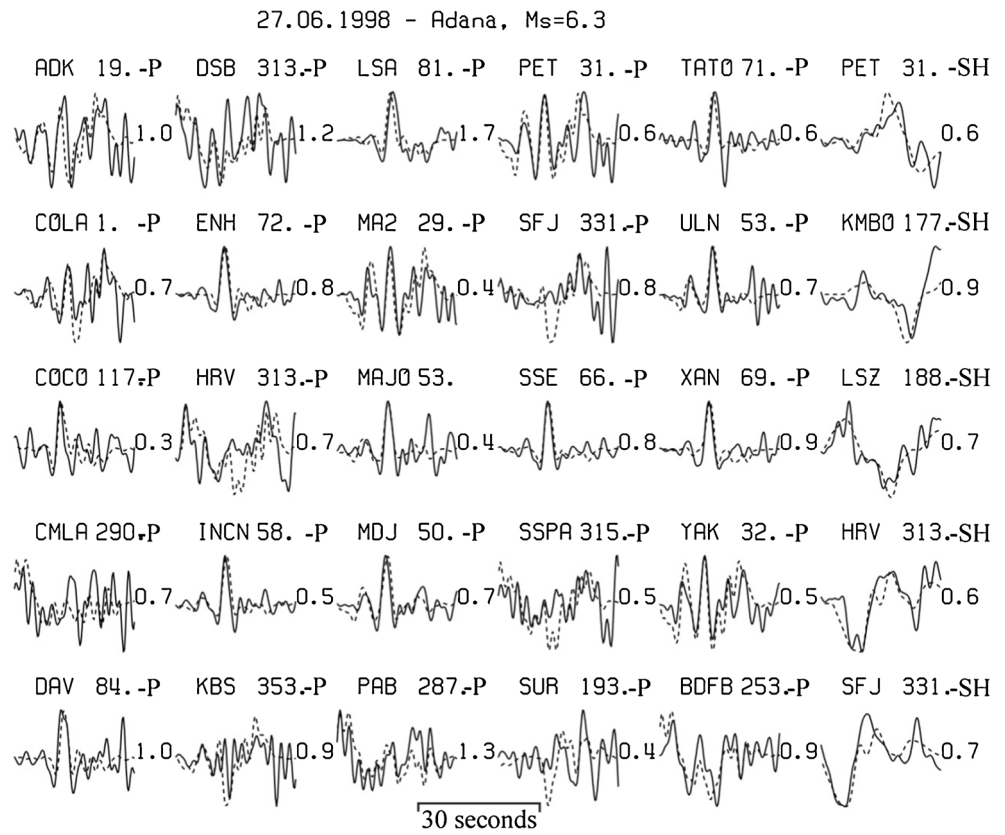


Fig. 7 3D schematic representation of the 1998 Adana earthquake's source region with the slip model obtained in the study is emplaced. See the caption of Fig. 3 for the abbreviations and referencing

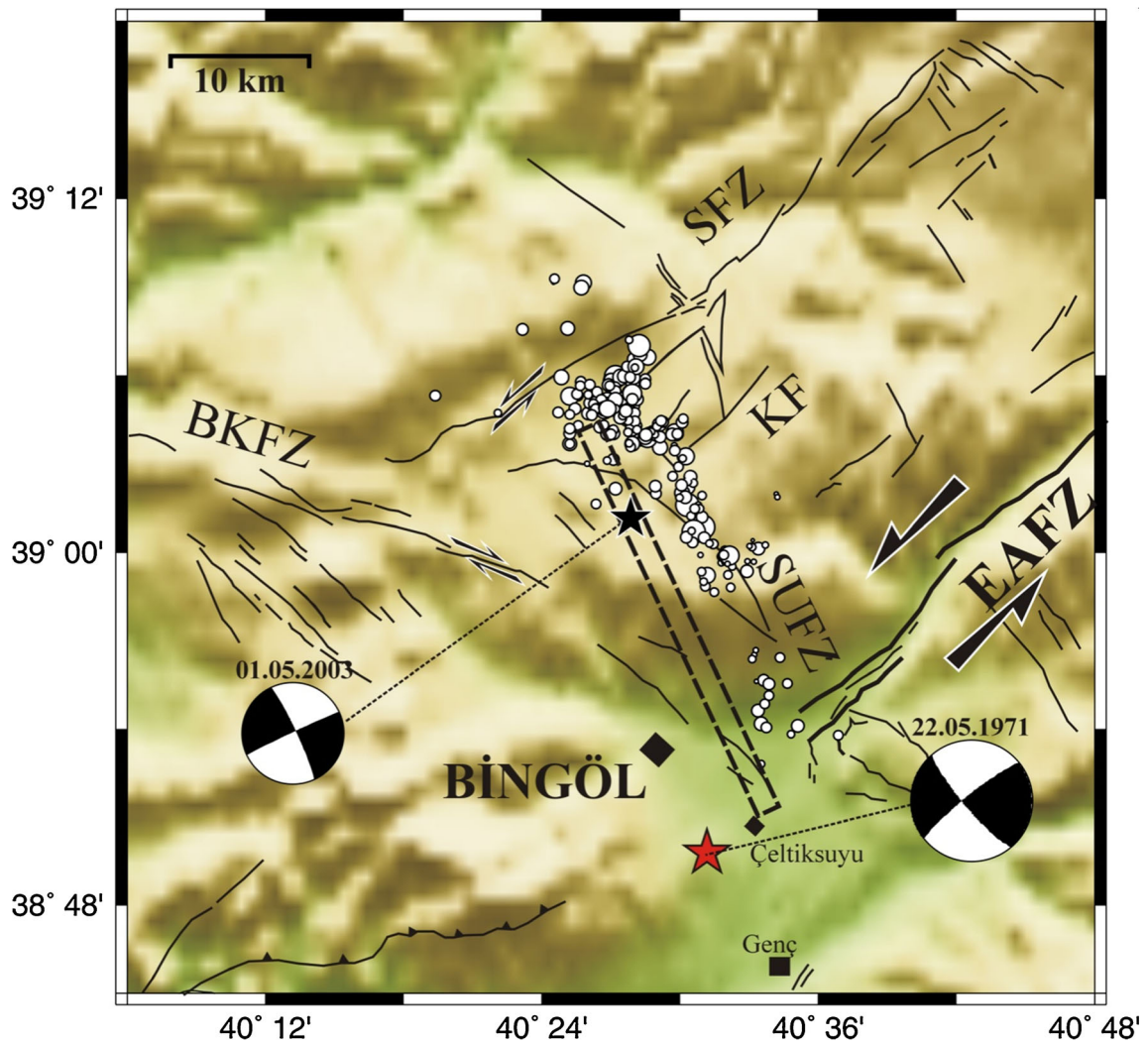


Fig. 8 Location map showing the epicenter (black star), the aftershocks (white circles), and fault plane solution of the 1 May 2003 Bingöl earthquake. The red star indicates the epicenter of the 1971 Bingöl earthquake ($M_s = 6.8$). Broken-line rectangle demonstrates the surface

projection of the model fault plane shown in Fig. 2b. Faults are adapted from Emre et al. (2013). *EAFZ* East Anatolian Fault Zone, *SFZ* Sancak–Uzunpınar Fault Zone, *SUFZ* Sancak–Uzunpınar Fault Zone, *BKFZ* Bingöl–Karakoçan Fault Zone, *KE* Kilisedere Fault

Table 4 The source parameters of the 1 May 2003 Bingöl earthquakes obtained by previous inversion studies and the seismological centers

	USGS	Harvard GCMT	KOERI ^a	Pınar 2003 ^b
				1st shock/2nd shock
Strike (°)	154 (334)	332		255/335
Dip (°)	90	68		55/84
Rake (°)	-178	-164		0/179
M_0 ($\times 10^{18}$ N-m)		4.09		
Latitude (°)	39.00	39.01	39.01	
Longitude (°)	40.44	40.53	40.45	
Depth (km)	10	15	10	

^a Kandilli Observatory and Earthquake Research Institute

^b From the inversion of the teleseismic *P* and *SH* waveforms (Pınar 2003, unpublished)

Table 5 Crustal velocity structure used in the inversion of the 1 May 2003 Bingöl earthquakes (modified from Kenar and Toksöz 1989)

Thickness (km)	V_p (km/s)	V_s (km/s)	ρ (kg/m ³)
5	4.60	3.00	2660
16	5.80	3.29	2750
20	7.00	3.89	2880
–	8.10	4.44	3300

Model fault parameterization

The rupture of the 2003 Bingöl earthquake is initially represented with a rectangular fault plane having dimensions of 30 km by 18 km, striking 335° and dipping 85° toward NE and divided into 60 square subfaults (Figs. 2b and 8, Table 4). The rake angle is firstly fixed at a value of -178° . The top edge of the fault plane lies over the earth surface and the bottom depth reaches virtually a depth of 18 km. The rupture initiates at the epicenter location determined by KOERI (39.01° N; 40.45° E) and intersects the fault plane at a depth of 10 km. Four time windows, slip-rise time of each represented by isosceles triangle of 0.2 s rise and fall and each lagged in time from the previous one by 0.4 s, to provide a total rise time of 1.6 s across the fault, are utilized. The crustal velocity structure in the source region is after Kenar and Toksöz (1989) (Table 5). The rupture velocity is initially set to 3.0 km/s. Following the initial parameterization, several inversion runs with varying parameters, such as strike and rake angles, hypocentral locations, and rupture velocities, are also carried out in order to obtain their values that better explain the data.

Inversion results

As it can be seen from the listed results of the inversion runs in Table 6, the data require pure dextral fault rupture that unilaterally propagated toward SE (strike angle of 335°) from a focus located at 10 km depth (Model IRB1 in Table 6). The data seems to be satisfactorily modeled by a fixed rake angle. Slip distribution model that reflects results of the IRB1 is shown in Fig. 9 and corresponding synthetic waveforms are compared with the observed ones in Fig. 10. The rupture seems to be dominated by an asperity located updip SE of the hypocenter with a peak slip slightly exceeding 55 cm, and released a seismic moment of 4.1×10^{18} N-m ($M_w \cong 6.4$).

Discussion

The major source area of the 1998 Adana earthquake was centered at depth of about 27 km, covering a circular area of 10 km in diameter with a peak slip of about 60 cm. The slip

NE of the major source decreases below 25 cm. The shallow minor slip at the NE top corner of the fault is most likely inversion artificial. The fault rupture is completely unilateral toward NE and covers a rectangular fault area that is 30 km in length. Observed heavy damage in Ceyhan town in the NE end of the fault plane supports unilateral rupture propagation toward NE (Fig. 7). The rupture is almost pure left lateral and the only largest slip area has a small dip slip component. Average rake angle for the slip model is about 10° . The inversions with fixed rake angles also indicate that the data prefer a rake angle smaller than 15° and greater than 0° (Table 3 and Fig. 4).

In the continental fault zones, the seismogenic zone is generally confined to the depths above 20 km and the lower crust has much lower seismic activity or deforms fully aseismically (Chen and Molnar 1983; Scholz 1988). Such a general rheology of the continental crust has been known as “jelly sandwich” model, which requires a brittle upper crust over a ductile lower crust overlying a strong uppermost mantle (Meissner and Kern 2008; Chen et al. 2013). These rheological differences are dictated by the temperature changes. The crustal earthquakes are limited to depth with temperatures 350 °C while temperature 700 °C marks depth of the upper mantle earthquake occurrences. If the temperatures are lower than the defined values or the entire crust is cooler than 350 °C and the temperature of 700 °C is not achieved in the uppermost mantle, then the earthquakes could also occur in the lower crust and uppermost mantle, which is known as “Caramel Slab” model of crustal rheology (Chen et al. 2013). Seismically active lower crust was also observed in some regions of the world where crustal thickening and lateral expulsion of crustal blocks are taking place and in areas with lower crustal lamination (Meissner and Kern 2008; Chen et al. 2013). For example, in the Tien Shan, Northern India, West Kunlun Range, and northern Alpine foreland, earthquakes occur within the full thickness of the continental crust to a depth of 40–45 km (Chen and Molnar 1983; Maggi et al. 2000; Huang et al. 2011; Mandal and Pandey 2011).

Our preferred inversion result indicates that the 1998 Adana earthquake’s rupture is confined to the depths below 15 km. An inversion run with a model fault cutting the depth range of 1–24.7 km or forcing a rupture in the upper crust with hypocentral depth of 22 km gave poor fit to the data (IRA8 in Table 3). This result coincides with the depth distribution of both well-constrained aftershocks of the 1998 Adana earthquake and the background seismicity which indicated main part of the earthquakes to occur in the depth range of 5–35 km (Ergin 1999; Aktar et al. 2000; Ergin et al. 2004), suggesting seismically active lower crust for the earthquake source region. This reckoning is not farfetched considering that the earthquake source region is located near the junction of the converging Arabian, African, and Anatolian plates which led to a relatively thick crust and a diffuse left-lateral shear zone

Table 6 Inversion results for different fault model parameterizations for the 2003 Bingöl earthquake

Trial	Fault dimensions (km)	Subfault	Distance from the SE edge (km)	Strike	Dip	Rake	Depth (km)	V_r (km/s)	$\ \mathbf{b} - \mathbf{Ax}\ $	M_0 ($\times 10^{18}$ N-m)
IRB1	30 × 18	60	23	335	84	-178	10	2.7	18.339	4.10
IRB2	30 × 18	60	15	335	84	-178	10	2.7	18.738	3.40
IRB3	30 × 18	60	7	335	84	-178	10	2.7	19.023	3.97
IRB4	30 × 18	60	23	335	84	-178	10	3.0	18.378	4.07
IRB5	30 × 18	60	23	335	84	-178	10	2.5	18.415	3.99
IRB6	30 × 18	60	23	335	84	-178	15	2.7	18.526	3.55
IRB7	30 × 18	60	23	335	84	-178	12	2.7	18.759	3.55
IRB8	30 × 18	60	23	320	84	-178	10	2.7	19.868	3.57
IRB9	30 × 18	60	23	335	84	-180	10	2.7	18.831	4.70
IRB910	30 × 18	60	23	335	84	-180 -190 -190	10	2.7	18.624	4.30

The value of $\|\mathbf{b} - \mathbf{Ax}\|$ indicates the Euclidean norm of the misfit between the synthetic and the observed data

(Ergin 1999). Additionally, it has been demonstrated that temperature gradients with depth derived from the wells in Adana basin are lower than the world average (Çoban 2008). This could be an indication of a cooler crust than the average, providing proper conditions for earthquake occurrence in the lower crust. It seems that “Caramel Slab” model is more suitable for the 1998 Adana earthquake.

As indicated above, both the mainshock and the aftershock locations require the mapped GYFZ to dip toward NW (strike angle of about 218°) in contrast to the source mechanisms plane solutions indicating a dip to SE and 15° difference in strike compared with the mapped GYFZ. An inversion trial (IRA9 in Table 3) with a rupture along the NW-dipping GYFZ significantly degraded fit to the data leading a conclusion that the earthquake might have occurred on an unmapped, SE-dipping splay fault of the GYFZ buried under the thick sediments of the Adana Basin with no indication over the surface (Fig. 3). The proposed fault could be southwest continuation of the Misis Fault mapped by Emre et al. (2013) within the GYFZ. This could be better understood from Fig. 7, where 3D

representation of the proposed source model for the 1998 Adana earthquake is demonstrated.

The rupture of the 2003 Bingöl earthquake almost confined to the depths above 10 km mainly proceeded to the SE from the hypocenter and covers a length of 20 km (Fig. 9). The large asperity alone covers a length of 10 km along the strike and its largest slip area centered at a depth of 5 km. There is also a smaller slip area down dip from the large asperity at a depth of 15 km. Fault parameterization requiring bilateral rupture and unilateral rupture toward NW gave poor fit to the data (trials IRB2 and IRB3 in Table 6). A unilateral rupture toward SE is apparent from the near source ground motion and compatible with the heavy damage and casualties in Bingöl city and Çeltiksuyu town located right over the SE end of the rupture (Yalçinkaya 2003; Dirik et al. 2003; Turer et al. 2004). The rupture initiating at 10 km depth has been defined to be a better assumption of the earthquake compared with the rupture starting at 12 and 15 km, indicating shallow rupture (Table 6). Since slip mainly occurred above the depth of 10 km and well-located aftershocks distributed mostly

Fig. 9 Co-seismic slip distribution model of the 1 May 2003 Bingöl earthquake obtained in the study. Slip is contoured at 5-cm intervals and only slips larger than 5 cm are contoured. The solid star demonstrates the hypocenter

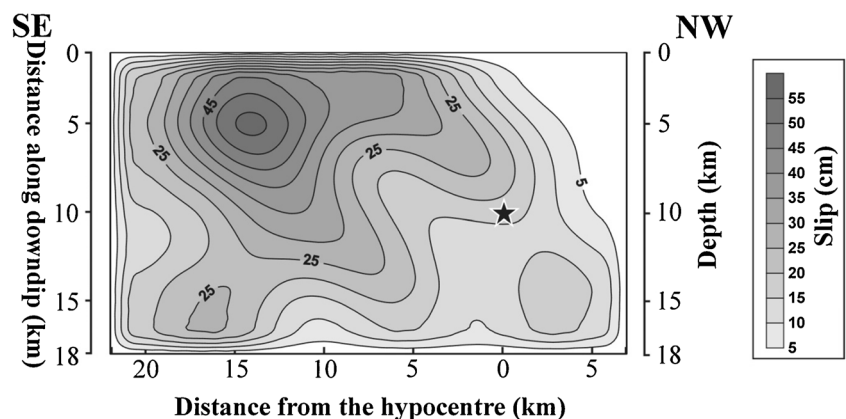


Fig. 10 Comparison of the predicted *P* and *SH* waveforms calculated for the slip model shown in Fig. 5 (dashed) with the observed waveforms (solid). See caption of Fig. 6 for the details of the figure

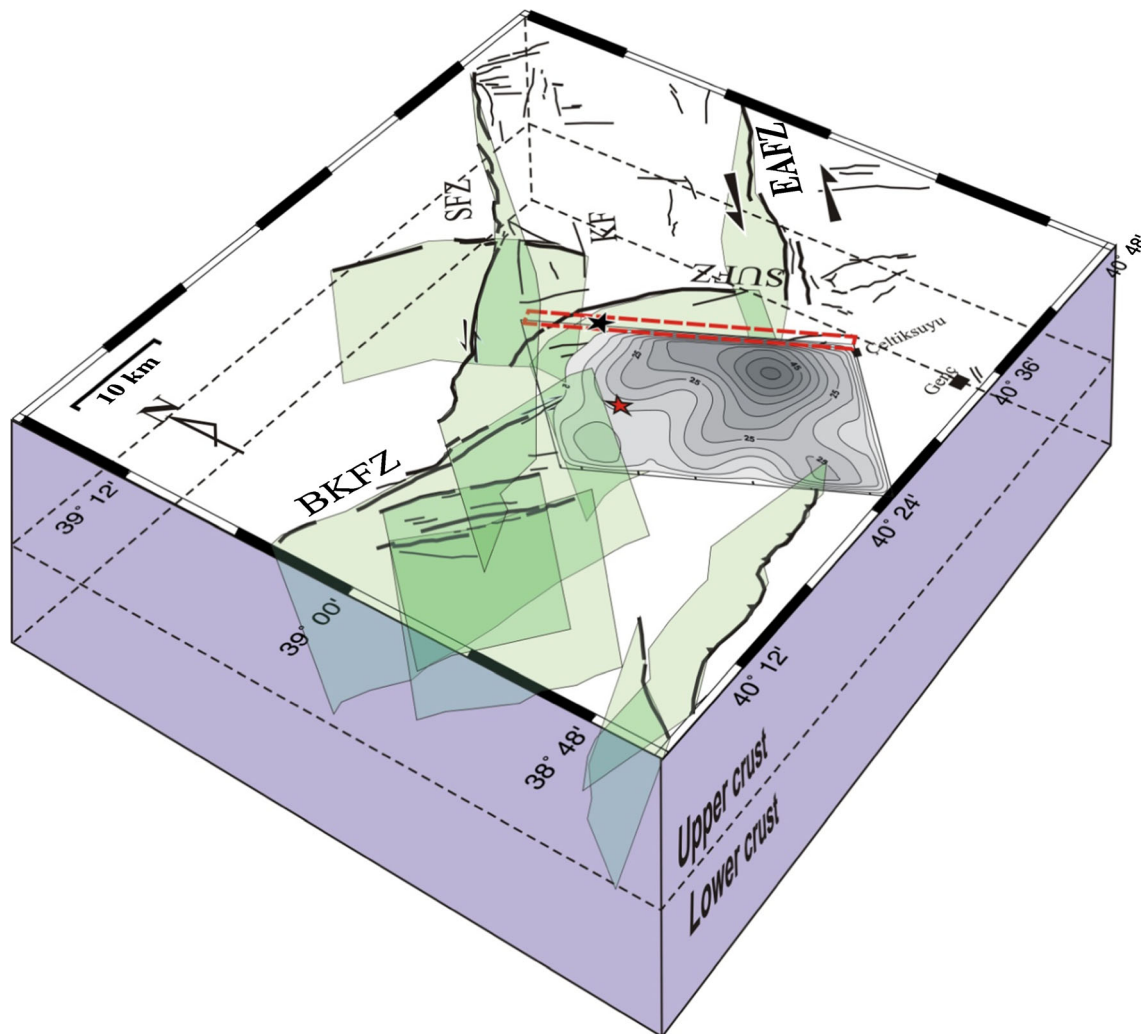
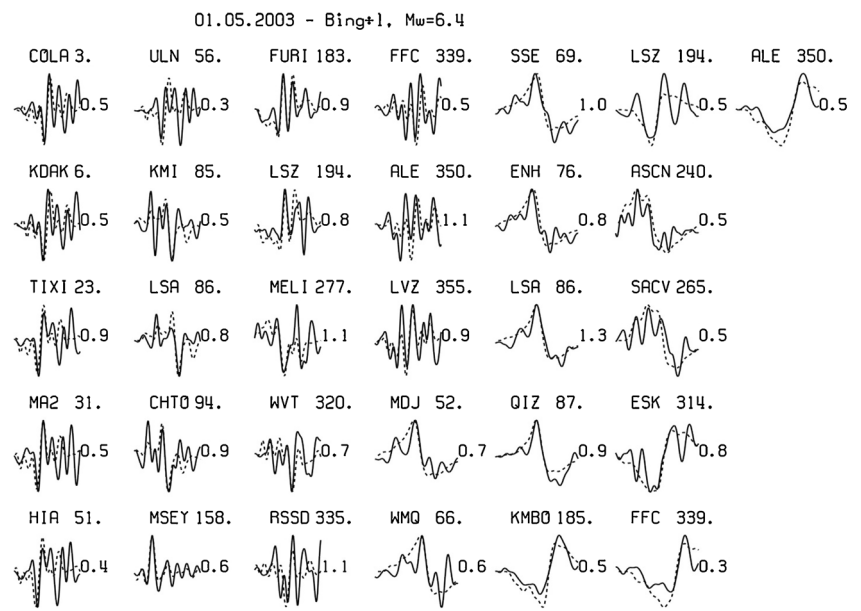


Fig. 11 3D schematic representation of the 2003 Bingöl earthquake's source region with the slip model obtained in the study is embedded. See the caption of Fig. 8 for the abbreviations and referencing

between depths of 3 and 14 km (Milkereit et al. 2004), the “jelly sandwich” model or a brittle upper crust and aseismic lower crust is the most suitable rheological model for the 2003 Bingöl earthquake. Tan et al. (2011) also indicated a seismogenic crust thickness of 15 km in Bingöl area.

It is interesting to note that although the main rupture was shallow, it supports the idea that discontinuous surface perturbations observed in the field (Dirik et al. 2003; Lazios et al. 2004) might be related to the faulting. As indicated above, the SUFZ has been proposed as the source fault because mapped discontinuous surface ruptures extend diffusely around its strike and it is the most probable candidate for the strike of the elongation defined by well-located aftershocks (Milkereit et al. 2004). However, seismological data indicates a strike 15° different from the general strike of the SUFZ, which has a strike of 320°. Figure 11, in which the slip model obtained in the study is shown within the 3D representation of the source region, apparently indicates the difference. Therefore, an inversion run with a fault model striking 320° has been carried out (trial IRB8 in Table 6). This parameterization significantly degraded fit to the data suggesting that the fault generated the earthquake might have been a different fault that is a splay fault of the SUFZ. Notice that a strike of 335° is also a better assumption for faulting regarding the elongation of the well-located aftershocks. From Fig. 11, it is also clear that the rupture of the 2003 Bingöl earthquake took place between the EAFZ and Kilisedere Fault suggesting not only prolongation of the source fault bifurcating from the SUFZ but also significance of the structural discontinuities in earthquake ruptures.

Conclusions

Teleseismic broadband *P* and *SH* body waveforms of both the 27 June 1998 Adana and the 1 May 2003 Bingöl earthquakes which occurred along the East Anatolian Fault Zone have been inverted to obtain finite-fault co-seismic slip distribution models. For the 1998 Adana earthquake, fixed-rake models fit the data less well than the variable-rake model, indicating the presence of a minor reverse component. The faulting was unilateral to the NE and confined to depths below 15 km for a length of 30 km along the strike (53°), dipping 81° SE. The main rupture located NE of the hypocenter was centered at a depth of about 27 km, covering a circular area of 10 km in diameter with a peak slip of about 60 cm. The slip model of the 1 May 2003 Bingöl earthquake indicated that the rupture was unilateral toward SE and was controlled by a failure of large asperity roughly circular in shape and centered at a depth of 5 km with peak displacement of about 55 cm. Obtained slip models suggest that both earthquakes might have occurred along unmapped faults with seismic moments more or less corresponding to $M_w \cong 6.4$ events.

Acknowledgements This research was funded by the Research Fund of the Sakarya University (project no. 2012-01-14-005).

References

- Aksu AE, Calon TJ, Hall J, Mansfield S, Yaşar D (2005) The Cilicia–Adana basin complex, eastern Mediterranean: Neogene evolution of an active fore-arc basin in obliquely convergent margin. *Mar Geol* 221:121–159
- Aksu AE, Walsh-Kennedy S, Hall J, Hiscott RN, Yaltrak C, Akhun SH, Çifçi G (2014) The Pliocene–Quaternary tectonic evolution of the Cilicia and Adana basins, eastern Mediterranean: special reference to the development of the Kozan Fault zone. *Tectonophysics* 622:22–43
- Aktar M, Ergin M, Özalaybey S, Tapırdamaz C, Yörük A, Biçmen F (2000) A lower-crustal event in the northeastern Mediterranean: the 1998 Adana earthquake (MW = 6.2) and its aftershocks. *Geophys Res Lett* 27:2361–2364
- Altunel E, Meghraoui M, Karabacak V, Akyüz SH, Ferry M, Yalçın Ç, Munsch M (2009) Archaeological sites (tell and road) offset by the dead sea fault in the Amik Basin, southern Turkey. *Geophys J Int* 179(3):1313–1329
- Ambraseys NN (1989) Temporary seismic quiescence: SE Turkey. *Geophys J Int* 96(2):311–331
- Ambraseys NN (2009) Earthquakes in the Mediterranean and Middle East: a multidisciplinary study of seismicity up to 1900. Cambridge University Press, Cambridge
- Arpacioğlu B (2000) Focal mechanism solution, moment tensor analysis and tectonic interpretation of 27.06.1998 Adana earthquake. MSc thesis, Kocaeli University
- Barka AA, Kadinsky-Cade K (1988) Strike-slip fault geometry in Turkey and its influence on earthquake activity. *Tectonics* 7(3):663–684
- Bulut F, Bohnhoff M, Eken T, Janssen C, Kılıç T, Dresen G (2012) The east Anatolian fault zone: seismotectonic setting and spatiotemporal characteristics of seismicity based on precise earthquake locations. *J Geophys Res-Sol Ea* 117. <https://doi.org/10.1029/2011JB008966>
- Burton-Ferguson R, Aksu AE, Calon AE, Hall J (2005) Seismic stratigraphy and structural evolution of Adana Basin, eastern Mediterranean. *Mar Geol* 221:189–222
- Chen WP, Molnar P (1983) Focal depths of intercontinental and intraplate earthquakes and their implications for the thermal and mechanical properties of the lithosphere. *J Geophys Res* 88:4183–4214
- Chen WP, Yu CQ, Tseng TL, Yang Z, Wang CY, Ning J, Leonard T (2013) Moho, seismogenesis, and rheology of the lithosphere. *Tectonophysics* 609:491–503
- Choy GL, Cormier VF (1986) Direct measurement of the mantle attenuation operator from broadband P and S waveforms. *J Geophys Res-Sol Ea* 91(B7):7326–7342
- Çoban K (2008) Temperature gradient distribution in Adana–İskenderun Neogene basins and its effects on hydrocarbon generation system. *Geosound* 53:1019–1003
- Derman AS, Gürbüz K (2007) Nature, provenance and relationships of Early Miocene Palaeovalley fills, northern Adana Basin, Turkey: their significance for sediment-bypassing on a carbonate shelf. *Turk J Earth Sci* 16:181–209
- Dirik K, Yürür T, Demirbağ AGH (2003) 1 Mayıs 2003 Çimenli (Bingöl) Depremi Değerlendirme Raporu. Hacettepe Üniversitesi Mühendislik Fakültesi Jeoloji Mühendisliği Bölümü, Temmuz 2003, Ankara, 31 sf (in Turkish)
- Duman TY, Emre Ö (2013) The east Anatolian fault: geometry, segmentation and jog characteristics. *Geol Soc En Lond Spec Publ* 372(1): 495–529
- Emre Ö, Herece E, Doğan A, Parlak O, Özaksoy V, Çıplak R, Özalp S (2003) 1 Mayıs 2003 Bingöl depremi değerlendirme raporu, Rapor No: 1085, Maden Tetkik Arama Genel Müdürlüğü, Ankara, 14 sf (in Turkish)

- Emre Ö, Duman TY, Özalp S, Elmacı H, Olgun Ş, Şaroğlu Ş (2013) Active fault map of Turkey with explanatory text 1:1.250.000 scale. General Directorate of Mineral Research and Exploration, Special Publication Series-30, Ankara, Turkey. ISBN: 978-605-5310-56-1
- Ergin M (1999) Present day seismicity and seismotectonic characteristics of the Cilician region. PhD thesis Istanbul Technical University, pp 312
- Ergin M, Aktar M, Eyidoğan H (2004) Present-day seismicity and seismotectonics of the Cilician Basin: eastern Mediterranean region of Turkey. *Bull Seismol Soc Am* 94(3):930–939
- Hartzell SH, Heaton TH (1983) Inversion of strong-ground motion and teleseismic wave form data for the fault rupture history of the 1979 Imperial Valley, California, earthquake. *Bull Seismol Soc Am* 73: 1553–1583
- Huang GCD, Roecker SW, Levin V (2011) Lower-crustal earthquakes in the west Kunlun range. *Geophys Res Lett* 38:L01314. <https://doi.org/10.1029/2010GL045893>
- Hubert-Ferrari A, King G, Manighetti I, Armijo R, Meyer B, Tapponnier P (2003) Long-term elasticity in the continental lithosphere: modelling the Aden ridge propagation and the Anatolian extrusion process. *Geophys J Int* 153(1):111–132
- Karig DE, Kozlu H (1990) Late Palaeogene–Neogene evolution of the triple junction near Maraş, south-Central Turkey. *J Geol Soc Lond* 147:1023–1034
- Kenar O, Toksöz N (1989) Dispersion and attenuation properties of surface waves in Anatolia. *Jeofizik* 3:92–106 (in Turkish)
- Langston CA, Helmberger DV (1975) A procedure for modelling shallow dislocation sources. *Geophys J Int* 42(1):117–130
- Lawson CL, Hanson RJ (1974) Linear least squares with linear inequality constraints. *Chap* 23:158–173
- Lazios S, Lekkas E, Danamos G (2004) The Bingöl, Eastern Turkey, Earthquake, Co-seismic Phenomena and Damage Distribution. 13th World Conference on Earthquake Engineering Paper No. 3010, Canada
- Maggi A, Jackson JA, Priestley K, Baker C (2000) A re-assessment of focal depth distributions in southern Iran, the Tien Shan and northern India: do earthquakes really occur in the continental mantle. *Geophys J Int* 143:629–661
- Mahmoud Y, Masson F, Meghraoui M, Cakir Z, Alchalbi A, Yavasoglu H, Yönlü O, Daoud M, Ergintav S, Inan S (2013) Kinematic study at the junction of the east Anatolian fault and the Dead Sea fault from GPS measurements. *J Geodyn* 67:30–39
- Mandal P, Pandey OP (2011) Seismogenesis of the lower crustal intraplate earthquakes occurring in Kachchh, Gujarat, India. *J Asian Earth Sci* 42:479–491
- McClusky S, Balassanian S, Barka A, Demir C, Ergintav S, Georgiev I, Gurkan O, Hamburger M, Hurst K, Kahle H, Kastens K, Kekelidze G, King R, Kotzev V, Lenk O, Mahmoud S, Mishin A, Nadariya M, Ouzounis A, Paradissis D, Peter Y, Prilepin M, Reilinger R, Sanli I, Seeger H, Tealeb A, Toksöz MN, Veis G (2000) Global positioning system constraints on plate kinematics and dynamics in the eastern Mediterranean and Caucasus. *J Geophys Res Solid Earth* 105(B3): 5695–5719
- McKenzie D (1972) Active tectonics of the Mediterranean region. *Geophys J Int* 30(2):109–185
- Meissner R, Kern H (2008) Earthquakes and strength in the laminated lower crust—can they be explained by the “corset model”? *Tectonophysics* 448(1):49–59
- Mendoza C (1995) Finite-fault analysis of the 1979 March 14 Petatlan, Mexico, earthquake using teleseismic P waveforms. *Geophys J Int* 121(3):675–683
- Milkereit C, Grosser H, Wang R, Wetzel HU, Woith H, Karakisa S et al (2004) Implications of the 2003 Bingöl earthquake for the interaction between the north and east Anatolian faults. *Bull Seismol Soc Am* 94(6):2400–2406
- Nalbant SS, McCloskey J, Steacy S, Barka AA (2002) Stress accumulation and increased seismic risk in eastern Turkey. *Earth Planet Sci Lett* 195(3):291–298
- Nalbant SS, McCloskey J, Steacy S (2005) Lessons on the calculation of static stress loading from the 2003 Bingöl, Turkey Earthquake. *Earth Planet Sci Lett* 235:632–640
- Pınar A (1995) Rupture process and spectra of some major Turkish earthquakes and their seismotectonic implications. PhD thesis, Bogazici University, Istanbul
- Pınar A, Honkura Y, Kuge K, Matsushima M, Sezgin N, Yılmaz M, Ögütçü Z (2007) Source mechanism of the 2000 November 15 Lake Van earthquake ($M_w = 5.6$) in eastern Turkey and its seismotectonic implications. *Geophys J Int* 170(2):749–763. <https://doi.org/10.1111/j.1365-246X.2007.03445.x>
- Reilinger R, McClusky S, Vernant P, Lawrence S, Ergintav S, Cakmak R, Ozener H, Kadirov F, Guliev I, Stepanyan R, Nadariya M, Hahubia G, Mahmoud S, Sakr K, ArRajehi A, Paradissis D, al-Aydrus A, Prilepin M, Guseva T, Evren E, Dmitrova A, Filikov SV, Gomez F, al-Ghazzi R, Karam G (2006) GPS constraints on continental deformation in the Africa–Arabia–Eurasia continental collision zone and implications for the dynamics of plate interactions. *J Geophys Res Solid Earth* 111
- Şaroğlu F, Emre O, Kusu I (1992) Active fault map of Turkey. General Directorate of Mineral Research and Exploration, Ankara
- Scholz C (1988) The brittle–plastic transition and the depth of seismic faulting. *Geol Rundsch* 77(1):319–328
- Şengör AMC, Tüysüz O, İmren C, Sakıncı M, Eyidoğan H, Görür N, le Pichon X, Rangin C (2005) The north Anatolian fault: a new look. *Annu Rev Earth Planet Sci* 33:37–112
- Seyrek A, Demir T, Westaway R, Guillou H, Scaillet S, White TS, Bridgland DR (2014) The kinematics of Central-Southern Turkey and Northwest Syria revisited. *Tectonophysics* 618:35–66
- Tan O, Pabuççu Z, Tapırdamaz MC, Inan S, Ergintav S, Eyidoğan H, Aksoy E, Kuluöztürk F (2011) Aftershock study and seismotectonic implications of the 8 March 2010 Kovancılar (Elazığ, Turkey) earthquake ($M_w = 6.1$). *Geophys Res Lett* 38:L11304. <https://doi.org/10.1029/2011GL047702>
- Taymaz T, Eyidoğan H, Jackson J (1991) Source parameters of large earthquakes in the east Anatolian fault zone (Turkey). *Geophys J Int* 106(3):537–550
- Toksöz MN, Nábělek J, Arpat E (1978) Source properties of the 1976 earthquake in East Turkey: a comparison of field data and teleseismic results. *Tectonophysics* 49(3–4):199–205
- Turer A, Yakut A, Uğurhan A (2004) Building damage patterns in Bingöl-Turkey after the May 1st, 2003 earthquake. In 13th World Conference on Earthquake Engineering, Paper (No. 65)
- Vernant P, Nilforoushan F, Hatzfeld D, Abbassi MR, Vigny C, Masson F, Nankali H, Martinod J, Ashtiani A, Bayer R, Tavakoli F, Chéry J (2004) Present-day crustal deformation and plate kinematics in the Middle East constrained by GPS measurements in Iran and northern Oman. *Geophys J Int* 157(1):381–398
- Wald DJ, Heaton TH (1994) Spatial and temporal distribution of slip for the 1992 Landers, California, earthquake. *Bull Seismol Soc Am* 84(3):668–691
- Wald DJ, Helmberger DV, Heaton TH (1991) Rupture model of the 1989 Loma Prieta earthquake from the inversion of strong-motion and broadband teleseismic data. *Bull Seismol Soc Am* 81(5):1540–1572
- Walsh-Kennedy S, Aksu AE, Hall J, Hiscott RN, Yaltrak C, Çiçi G (2014) Source to sink: the development of the latest Messinian to Pliocene–Quaternary Cilicia and Adana basins and their linkages with the outland Mut Basin, eastern Mediterranean. *Tectonophysics* 622:1–21
- Westaway R (2004) Kinematic consistency between the Dead Sea fault zone and the Neogene and Quaternary left-lateral faulting in SE Turkey. *Tectonophysics* 391(1):203–237
- Yalçınkaya E (2003) 1 Mayıs 2003 Bingöl depremi ($M_w = 6.4$) kuvvetli hareket kayıtlarının incelenmesi. *Yerbilimleri* 28:99–108